

ORIGINAL ARTICLE

Magnetic resonance imaging of tumor necrosis

TORMOD A. M. EGELAND, JON-VIDAR GAUSTAD, KANTHI GALAPPATHI
& EINAR K. ROFSTAD*Group of Radiation Biology and Tumor Physiology, Department of Radiation Biology, Institute for Cancer Research, Oslo University Hospital, Oslo, Norway***Abstract**

Background. The prognostic and predictive value of magnetic resonance (MR) investigations in clinical oncology may be improved by implementing strategies for discriminating between viable and necrotic tissue in tumors. The purpose of this preclinical study was to investigate whether the extent of necrosis in tumors can be assessed by dynamic contrast-enhanced magnetic resonance imaging (DCE-MRI) and/or T_2 -weighted MR imaging. **Material and methods.** Three amelanotic human melanoma xenograft lines differing substantially in tumor necrotic fraction, necrotic pattern, extracellular volume fraction, and blood perfusion were used as experimental models of human cancer. MRI was performed at 1.5 T and a spatial resolution of $0.23 \times 0.47 \times 2.0 \text{ mm}^3$. Gadolinium diethylene-triamine penta-acetic acid (Gd-DTPA) was used as contrast agent. Plots of Gd-DTPA concentration versus time were generated for each voxel, and three parameters were calculated for each curve: the extracellular volume fraction (v_e), the final slope (a), and the Gd-DTPA concentration at one minute after the contrast administration ($C_{1\text{min}}$). Parametric images of v_e , a , $C_{1\text{min}}$, and the signal intensity in T_2 -weighted images (SI_{T_2W}) were compared with the histology of the imaged tissue. **Results.** The v_e , a , and $C_{1\text{min}}$ frequency distributions were significantly different for necrotic and viable tissue in all three tumor lines. By using adequate values of v_e , a , and $C_{1\text{min}}$ to discriminate between necrotic and viable tissue, significant correlations were found between the fraction of necrotic tissue assessed by MRI and the fraction of necrotic tissue assessed by image analysis of histological preparations. On the other hand, the SI_{T_2W} frequency distributions did not differ significantly between necrotic and viable tissue in two of the three tumor lines. **Conclusion.** Necrotic regions in tumor tissue can be identified in parametric images derived from DCE-MRI series, whereas T_2 -weighted images are unsuitable for detection of tumor necrosis.

The microvasculature of most malignant tumors shows severe morphological and architectural abnormalities, and these abnormalities result in inadequate and heterogeneous blood supply and the development of regions with necrotic tissue [1]. Histological examinations have revealed that the pattern of necrosis can differ substantially among individual tumors resected from the same organ. Some tumors show a few large necrotic regions centrally, whereas others develop many small necrotic foci throughout the tissue [2,3]. Necrotic tumor regions do not represent a therapeutic problem, but may confound biological and physiological studies of malignant tissues [4]. Moreover, the development of necrosis in malignant tissues after treatment may provide information on tumor treatment response [5]. A non-invasive method for assessing

the fraction of necrotic tissue in tumors is therefore highly warranted.

Several magnetic resonance (MR) techniques have been used to detect tumor necrosis, including dynamic contrast-enhanced imaging, T_2 -weighted spin echo imaging, diffusion weighted imaging, phosphorous spectroscopy, and contrast-enhanced imaging with contrast agents showing high affinity for necrotic tissue [6–11]. However, the usefulness of these strategies is uncertain as detailed comparative MR and histological studies investigating their general validity are sparse.

The potential of gadolinium diethylene-triamine penta-acetic acid (Gd-DTPA)-based dynamic contrast-enhanced magnetic resonance imaging (DCE-MRI) for characterizing the physiological microenvironment of tumors is currently being investigated in our

laboratory by using human tumor xenografts as pre-clinical models of human cancer [12–17]. In these studies, images of K^{trans} (the volume transfer constant of Gd-DTPA) and v_e (the extracellular volume fraction of the imaged tissue) are obtained by subjecting DCE-MRI series to pharmacokinetic analysis using the modified Kety model developed by Tofts et al. [18]. We have shown that our experimental procedure produces highly reproducible parametric images of K^{trans} and v_e [12,15] and that the numerical values of $E \cdot F$ (a K^{trans} -related parameter) and v_e are closely related to the absolute values of blood perfusion and extracellular volume fraction in the viable tissue regions of human melanoma xenografts [16]. Furthermore, even though the Tofts pharmacokinetic model is not valid for necrotic tissue, our algorithms produce very low K^{trans} values for voxels in tumor regions with extensive necrosis, consistent with the assumption of no blood perfusion in necrotic tissue [16]. The main purpose of the study reported here was to investigate whether the fraction of necrotic tissue in tumors can be assessed accurately by DCE-MRI and/or T_2 -weighted MR imaging. The study was based on previous work in our laboratory having suggested that pharmacokinetic analysis of DCE-MRI series may produce unphysiological values for v_e in tumor necroses [17] and that tumor necroses may show shorter T_2 values than viable tissue [7]. Three human melanoma xenograft lines differing substantially in necrotic fraction, necrotic pattern, extracellular volume fraction, and blood perfusion were used as tumor models.

Material and methods

Tumor models

T-22, V-27, and Z-98 human melanoma xenografts growing in adult (8–12 weeks of age) female BALB/c *nu/nu* mice were used as tumor models. Tumors were initiated from established cell lines cultured in RPMI-1640 (25 mM HEPES and L-glutamine) supplemented with 13% bovine calf serum, 250 mg/l penicillin, and 50 mg/l streptomycin. Approximately 5×10^5 cells in 10 μ l of Hanks' balanced salt solution were inoculated intradermally in the mouse leg. The mice were kept under specific pathogen-free conditions and were given sterilized food and tap water ad libitum. Experiments were initiated when the tumors had grown to a volume of 100–600 mm³. Tumor volume (V) was calculated as $V = \pi/6 \times a \times b^2$, where a is the longer and b is the shorter of two perpendicular diameters. MR imaging was carried out with anesthetized mice. Fentanyl citrate (Janssen Pharmaceutica, Beerse, Belgium), fluanisone (Janssen Pharmaceutica), and midazolam (Hoffmann-La Roche, Basel, Switzerland) were administered intraperitoneally

in doses of 0.63 mg/kg, 20 mg/kg, and 10 mg/kg, respectively. Animal care and experimental procedures were approved by the Institutional Committee on Research Animal Care and were performed in accordance with the Interdisciplinary Principles and Guidelines for the Use of Animals in Research, Marketing, and Education (New York Academy of Sciences, New York, NY).

Contrast agent

Gd-DTPA (Schering, Berlin, Germany), diluted in 0.9% saline to a final concentration of 0.06 M, was used as contrast agent. The contrast agent was administered in the tail vein of the mice in a bolus dose of 5.0 ml/kg. The administration was performed after the mice had been placed in the MR scanner by using a 24G-neoflon connected to a syringe by a polyethylene tubing.

MRI

MRI was performed with a 1.5-T whole-body scanner (Signa, General Electric, Milwaukee, WI) and a cylindrical slotted tube resonator transceiver coil constructed for mice [12,17]. The coil was insulated with styrofoam to prevent excessive heat loss from the mice. The body core temperature of the mice was kept at 37–38°C during imaging by using a thermostatically regulated heating pad. Two calibration tubes, one with 0.5 mM Gd-DTPA in 0.9% saline and the other with 0.9% saline only, were placed adjacent to the mice in the coil. The mice were placed in the scanner with the tumor in the isocenter, and the tumors were imaged axially in a single scan through the tumor center. A scan thickness of 2 mm was used, and the number of excitations was one. The image matrix was 256×64 with a field of view of 6×3 cm², corresponding to a voxel size of $0.23 \times 0.47 \times 2.0$ mm³. Interpolation algorithms applied by the imaging system resulted in an apparent resolution of $0.23 \times 0.23 \times 2.0$ mm³.

DCE-MRI series consisting of two types of spoiled recalled gradient images were recorded: proton density images with TR = 900 ms, TE = 3.2 ms, and $\alpha = 20^\circ$, and T_1 -weighted images with TR = 200 ms, TE = 3.2 ms, and $\alpha = 80^\circ$. Two proton density images and three T_1 -weighted images were acquired before the contrast agent was administered. The durations of the sequences were 64 s and 14 s, respectively. After the administration of contrast agent, T_1 -weighted images were recorded every 14 s for 15 min. Finally, two proton density image were acquired. Prior to the DCE-MRI, T_2 -weighted signal intensity images were recorded by using a spin echo sequence with TR = 5000 ms and TE = 65 ms.

The strengths and weaknesses of our MRI methods have been discussed in great detail in several previous reports [13,14,16].

Image processing and data analysis

Tumor images were stored in the DICOM format and analyzed by using in-house-made software developed in IDL (Interactive Data Language, Boulder, CO). Gd-DTPA concentrations were calculated from signal intensities as described by Hittmair et al. [19]. Curves for Gd-DTPA concentration versus time were generated for each voxel, and three parameters were calculated for each curve: the extracellular volume fraction (v_e) was calculated by using the arterial input function determined by Benjaminsen et al. [12] and the Tofts pharmacokinetic model [18] as described earlier [14,17], the final slope (a) was calculated by linear regression analysis using the five last minutes of the recordings, and the concentration of Gd-DTPA in the tumor tissue at one minute after the Gd-DTPA administration ($C_{1\text{min}}$) was calculated as the mean of the measurements recorded 45–75 s after the contrast administration. Images of v_e , a , $C_{1\text{min}}$, and the signal intensity in T_2 -weighted images (SI_{T_2W}) were generated by using the SigmaPlot software (SPSS Science, Chicago, IL).

Assessment of fraction of necrotic tissue

Histological sections were prepared from the tumors subjected to MRI for assessment of the fraction of necrotic tissue. To ensure that the histological sections matched the MR scans, we marked off the central axial scan on the tumors with a felt-tip pen and euthanized the mice immediately after imaging. The tumors were then cut into two halves along the middle of the scan, resected, and fixed in phosphate-buffered 4% paraformaldehyde. Three to six histological sections, separated by $\sim 400\ \mu\text{m}$, were cut from the central axial plane of each tumor, corresponding to the 2-mm-thick MR scan. The histological sections were stained with hematoxylin and eosin using standard procedures. The fraction of necrotic tissue (i.e., the area fraction showing necrotic tissue) was determined by subjecting the histological sections to image analysis [17].

Statistical analysis

Statistical comparisons of data were performed by using the Student's t -test when the data complied with the conditions of normality and equal variance. Under other conditions, comparisons were carried out by nonparametric analysis using the Mann-Whitney rank-sum test. The Kolmogorov-Smirnov

method was used to test for normality. The Bonferroni method was used to correct for multiple comparisons. Comparisons of pooled frequency distributions were based on the median values of the underlying single frequency distributions. Correlations between two parameters were searched for by linear regression analysis. Probability values (p) and correlation coefficients (R^2) were calculated by using the SigmaStat statistical software (SPSS Science). A significance criterion of $p < 0.05$, determined from two-sided test, was used.

Results

A total of 12 T-22 tumors, 14 V-27 tumors, and 11 Z-98 tumors were subjected to MRI and subsequent histological examination. The necrotic pattern differed substantially among the tumor lines (Figure 1a). The T-22 tumors showed several small necroses distributed throughout the tissue, most V-27 tumors had a large central necrosis, and the Z-98 tumors exhibited one or more medium-sized necrotic regions, frequently with islands of viable tissue within the necroses.

The curves for Gd-DTPA concentration versus time differed substantially between voxels in necrotic tissue and voxels in viable tissue in all tumor lines (Figure 1b). Voxels in viable tissue generally showed curves with a clear maximum, consistent with rapid uptake and slow washout of Gd-DTPA. In the vast majority of the voxels, the maximum occurred within the first 10 minutes of the recordings, and was followed by a linear decrease in the Gd-DTPA concentration. In contrast, the curves for most voxels in necrotic tissue were nearly linear during the whole imaging period, consistent with slow diffusion of Gd-DTPA into the necrotic tissue from the surrounding viable tissue. By calculating the final slopes of the curves from the five last minutes of the recordings, we hypothesized that the numerical value of a would be negative for most voxels in viable tissue and positive for most voxels in necrotic tissue. Furthermore, based on these Gd-DTPA uptake curves, we hypothesized that $C_{1\text{min}}$ would discriminate well between viable and necrotic tissue and clearly better than the maximum Gd-DTPA concentration.

To investigate whether necrotic tumor regions were identifiable in parametric MR images, images of v_e , a , $C_{1\text{min}}$, and SI_{T_2W} were compared with histological preparations from the imaged tissue. One example is illustrated in Figure 2, which shows a histological image and the corresponding parametric MR images of a representative V-27 tumor. In general, large necroses were easily recognizable in v_e , a , and $C_{1\text{min}}$ images, whereas SI_{T_2W} images depicted necrotic regions less clearly.

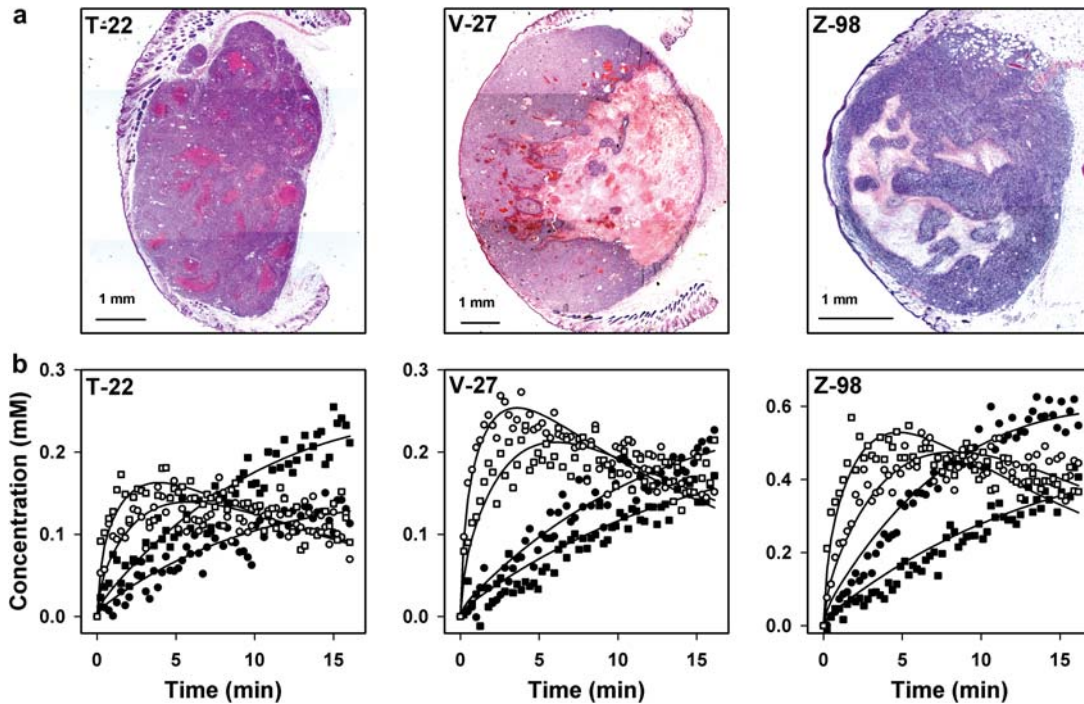


Figure 1. Histological images (a) and plots of Gd-DTPA concentration versus time for single voxels located in necrotic (●,■) or viable (○,□) tissue (b) of representative T-22, V-27, and Z-98 tumors.

To investigate whether the numerical values of v_e , a , $C_{1\min}$, and SI_{T2W} differed between necrotic and viable tissue, v_e , a , $C_{1\min}$, and SI_{T2W} frequency distributions were determined for tumor regions consisting of necrotic tissue only and tumor regions consisting of viable tissue only (Figure 3). Each of the frequency distributions in Figure 3 is based on five tumor regions, identified by examining all histological preparations from an imaged tissue. The v_e frequency distributions for viable tissue differed among the tumor lines ($p < 0.01$), and the numerical values were similar to those typical for the extracellular volume fraction of tumors. On the other hand, unphysiological v_e values were achieved for large fractions of the voxels in necrotic tissue. The parameter a had a negative value for most voxels in viable tissue and a positive value for the majority of the voxels in necrotic tumor regions, consistent with our hypothesis. $C_{1\min}$ had a positive value for the voxels in viable tissue and was close to zero for most voxels in necroses. The v_e , a , and $C_{1\min}$ frequency distributions were significantly different for necrotic and viable tissue in all three tumor lines ($p < 0.01$). However, despite these differences, the overlap was substantial regardless of whether v_e , a , or $C_{1\min}$ was considered. The frequency distributions for SI_{T2W} on the other hand, did not differ between necrotic and viable tissue in T-22 and Z-98 tumors ($p > 0.05$), but the SI_{T2W} values were significantly higher for viable than for necrotic tissue in V-27 tumors ($p < 0.05$).

The frequency distributions in Figure 3 suggested that voxels in viable tissue have v_e values below 0.15 (T-22), 0.35 (V-27), or 0.45 (Z-98), a values below $0.1 \text{ mM}\cdot\text{s}^{-1}$ (T-22, V-27) or $0.15 \text{ mM}\cdot\text{s}^{-1}$ (Z-98), $C_{1\min}$ values above 0.05 mM (T-22) or 0 mM (V-27, Z-98), and SI_{T2W} values between 12000 and 17500 (T-22), 7000 and 25000 (V-27), or 11000 and 22000 (Z-98). To investigate whether the fraction of voxels with v_e , a , $C_{1\min}$, or SI_{T2W} values outside these threshold values (NF_{MRI}) reflected the fraction of necrotic tissue as assessed by histological examination (NF_{hist}), plots of NF_{MRI} versus NF_{hist} were generated for each MR parameter (Figure 4). Linear correlations were found between NF_{MRI} and NF_{hist} for both v_e ($p < 0.0001$; $R^2 = 0.59$), a ($p < 0.0001$; $R^2 = 0.51$), $C_{1\min}$ ($p < 0.0001$; $R^2 = 0.43$), and SI_{T2W} ($p = 0.0017$; $R^2 = 0.25$). The correlation between NF_{MRI} and NF_{hist} for v_e was consistent with a one-to-one correlation, whereas NF_{hist} was underestimated by NF_{MRI} for a , $C_{1\min}$, and SI_{T2W} .

The one-to-one correlation between NF_{MRI} and NF_{hist} for v_e in Figure 4 was achieved by using different v_e threshold values for the different tumor lines. To investigate whether significant correlations between NF_{MRI} and NF_{hist} could be achieved by using the same v_e threshold value for all tumor lines, plots of NF_{MRI} versus NF_{hist} were generated for v_e threshold values of 0.15, 0.35, and 0.45 (i.e., the optimal v_e threshold value for T-22, V-27, and Z-98 tumors, respectively). However, each of these threshold values resulted in NF_{MRI}

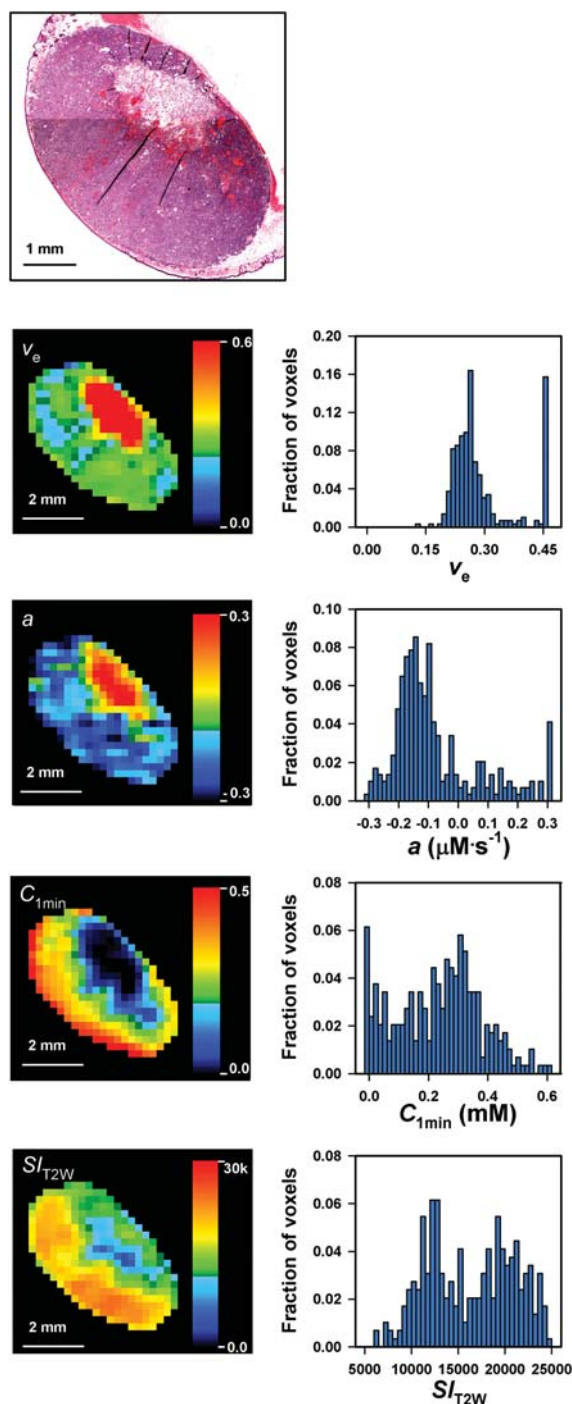


Figure 2. A histological image and parametric MR images and frequency distributions of v_e , a , C_{1min} , and SI_{T2W} for a representative V-27 tumor.

values that were either significantly higher or significantly lower than NF_{hist} for at least one of the tumor lines (Figure 5).

Discussion

Several institutions are attempting to develop biomarkers and predictive assays for the outcome of

treatment of cancer patients based on DCE-MRI [20,21]. Moreover, DCE-MRI is being used to monitor the response to treatment of cancer patients [22]. The prognostic value of DCE-MRI and its usefulness in prediction and monitoring of tumor treatment response may be improved substantially by implementing adequate methods for differentiating between necrotic and viable tissue.

In the present work, the T-22, V-27, and Z-98 melanoma xenograft lines were used as preclinical models to investigate whether the fraction of necrotic tissue in tumors can be assessed by DCE-MRI and/or T_2 -weighted imaging. These lines differ substantially in tumor necrotic fraction, pattern of necrosis, extracellular volume fraction, and blood perfusion and should thus be suitable models for elucidating the questions addressed in the present study. However, the tumor lines were of the same histological type and, consequently, it may be necessary to perform similar experiments with xenografted tumors of other histologies to investigate the general validity of our conclusions.

Parametric images of v_e , a , C_{1min} , and SI_{T2W} were generated and compared with the histology of the imaged tissue. These parameters were selected because parameters related to a , C_{1min} , and SI_{T2W} are being used to identify necrotic regions in preclinical and clinical studies without experimental verification of their validity as adequate measures of tumor necrosis [23–25]. Significant correlations between NF_{MRI} and NF_{hist} were found for all four parameters. However, there are weaknesses associated with each of these parameters since none of them provided distinctly different numerical values for necrotic and viable tissue.

Voxels with unphysiological v_e values colocalized with necrotic regions in histological sections, and the fraction of voxels with v_e values higher than those found in viable tissue showed a strong one-to-one correlation with NF_{hist} . However, a one-to-one correlation between NF_{MRI} and NF_{hist} required the use tumor line-specific threshold values for the upper limit of v_e in viable tissue. The use of common threshold v_e values, on the other hand, resulted in NF_{hist} being significantly overestimated or significantly underestimated by NF_{MRI} in at least one of the tumor lines, most likely because the extracellular volume fraction of the viable tissue differed significantly among the tumor lines. These observations suggest that the fraction of voxels with unphysiological v_e values is an excellent parameter for the fraction of necrotic tissue in experimental tumors, where the upper limit of the v_e of viable tissue can be determined easily. However, since the fraction of voxels with unphysiological v_e values is sensitive to this threshold v_e value, the usefulness of the fraction of voxels with unphysiological v_e

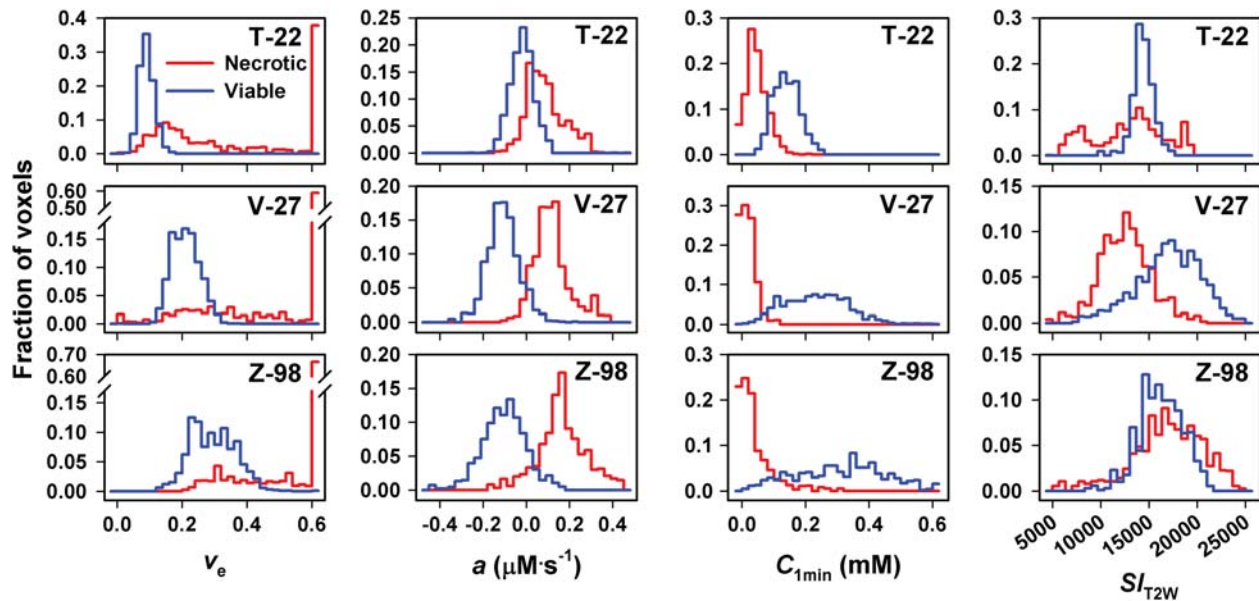


Figure 3. Frequency distributions of v_e , a , C_{1min} , and SI_{T2W} for viable and necrotic tissue in T-22, V-27, and Z-98 tumors. Each frequency distribution represents pooled data from five tumor regions.

values as a parameter for tumor necrosis may be limited in clinical DCE-MRI.

Moreover, NF_{MRI} showed significant correlations to NF_{hist} both when the fraction of voxels with a values higher than those found in viable tissue and when the fraction of voxels with C_{1min} values lower than those found in viable tissue were used as parameters for NF_{MRI} . The correlations were found to be insensitive to the exact time interval used for the calculation of a as long as the starting point of the regression analysis was beyond the time point where the majority of the voxels in viable tissue had their maximum value and the time interval was sufficiently long that the outcome of the regression analysis was not influenced significantly by noise, and insensitive to the exact time point used for assessing the concentration of Gd-DTPA as long as it was early in the observation period, but sufficiently late to have a significant uptake of Gd-DTPA in the viable tissue. However, although significant correlations were found, NF_{hist} was underestimated by NF_{MRI} for both parameters of NF_{MRI} , primarily because a significant proportion of the voxels in necrotic tissue showed a values and C_{1min} values similar to those found in viable tissue. Typically, low a values and high C_{1min} values were found in small necroses and in the periphery of large necroses, probably because Gd-DTPA diffused into necrotic tissue from the surrounding viable tissue [17]. Furthermore, it is also possible that NF_{MRI} underestimated NF_{hist} because a large proportion of the voxels consisting of a mixture of necrotic and viable tissue may have shown low a values and/or high C_{1min} values.

T-22 and Z-98 tumors showed SI_{T2W} frequency distributions that were not significantly different for necrotic and viable tissue. Consequently, necrotic regions cannot be detected in T_2 -weighted images of tumors similar to the T-22 and Z-98 tumors studied here.

The MRI was carried out by using a voxel size of $0.23 \times 0.47 \times 2.0 \text{ mm}^3$. This voxel size is large compared with the size of many necrotic structures, implying that a significant proportion of the voxels contained a mixture of viable and necrotic tissue. It is thus possible that any correlation between NF_{MRI} and NF_{hist} would be improved by increasing the spatial resolution of the MRI. An increased spatial resolution would probably make it possible to detect a larger number of small necroses and, hence, would be particularly beneficial in examinations of tumors with many small necrotic foci scattered throughout the tissue. Furthermore, an increased spatial resolution would probably improve the delineation of large necrotic regions in any parametric MR image of tumors. However, the spatial resolution used here is similar to or higher than that commonly used in clinical MRI [20–22] and, hence, the present observations should be clinically relevant.

Several investigators have suggested that tumor necrosis can be detected by diffusion-weighted [8] or T_1 -weighted [26] MRI. These possibilities have been investigated earlier in our laboratory by using melanoma xenografts as tumor models [7,27]. The apparent diffusion coefficient (ADC) was found to correlate well with the fraction of necrotic tissue in D-12 tumors but not in U-25 tumors, suggesting

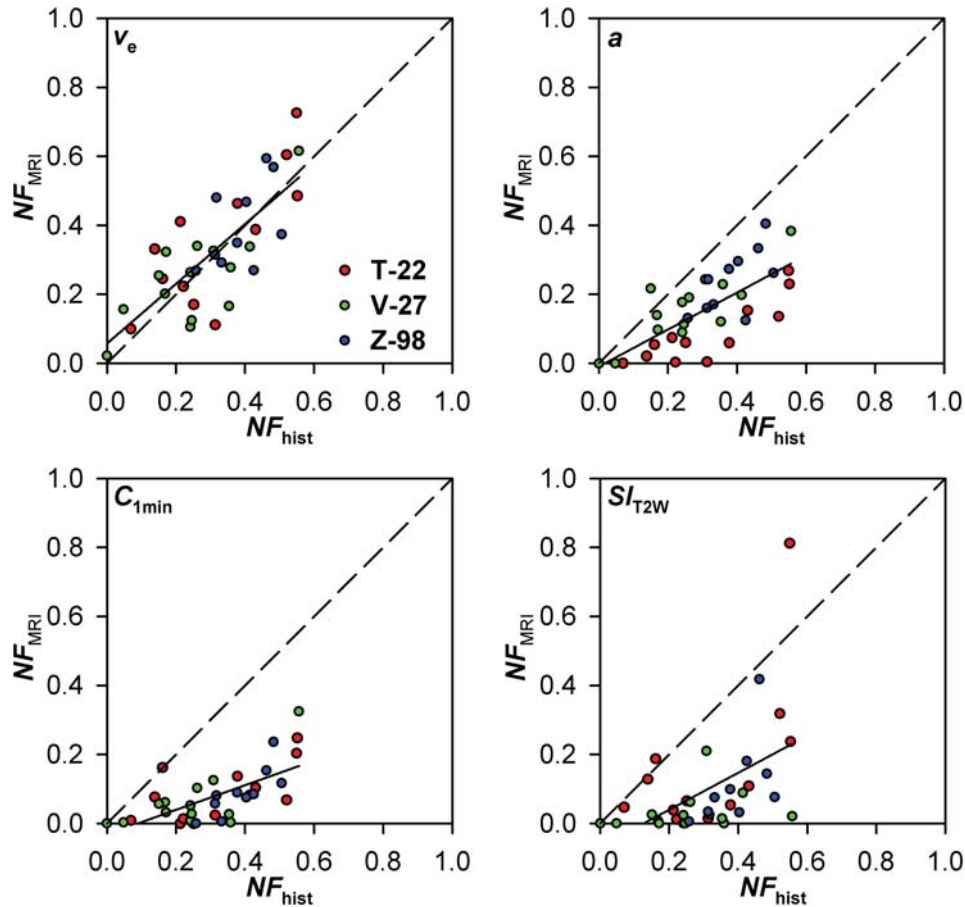


Figure 4. Fraction of necrotic tissue assessed by MRI (NF_{MRI}) versus fraction of necrotic tissue assessed by histological analysis (NF_{hist}) for T-22, V-27, and Z-98 tumors. NF_{MRI} refers to the fraction of voxels with numerical values of v_e , a , C_{1min} , and SI_{T2W} outside those detected in viable tissue in each of the tumor lines. The solid lines were fitted to the data by regression analysis. The dashed lines represent theoretical one-to-one correlations.

that ADC maps may be used to quantify necrosis in some but not in all experimental tumors [27]. T_1 was found to be shorter in the necrotic tissue than in the surrounding viable tissue of BEX-t, HUX-t, and SAX-t tumors, but the delineation of the necroses in T_1 -weighted and pure T_1 images did not corre-

spond well to the histological appearance of the necroses [7].

In summary, our preclinical study suggests that tumor necrosis can be identified accurately in v_e images provided that the upper limit of the v_e of the viable tissue can be determined. Furthermore, tumor

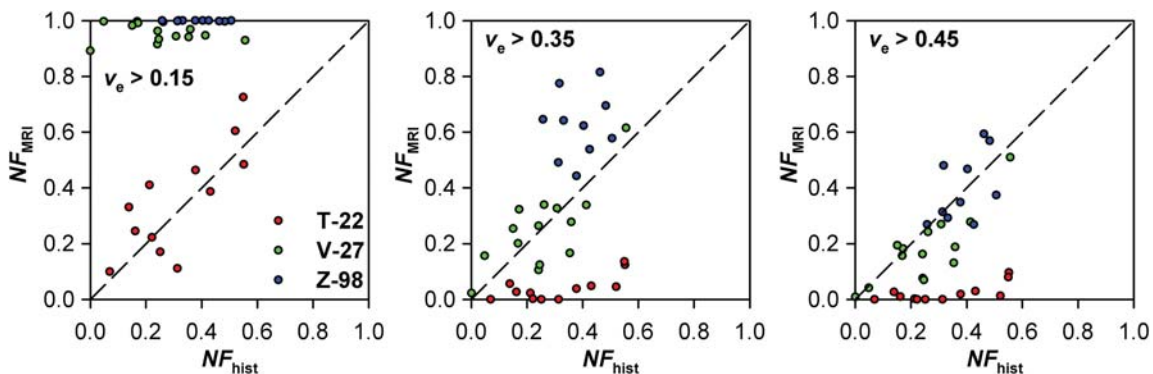


Figure 5. Fraction of necrotic tissue assessed by MRI (NF_{MRI}) versus fraction of necrotic tissue assessed by histological analysis (NF_{hist}) for T-22, V-27, and Z-98 tumors. NF_{MRI} refers to the fraction of voxels with v_e values > 0.15 , 0.35 , and 0.45 . The dashed lines represent theoretical one-to-one correlations.

necrosis can also be detected in images of a and C_{min} related parameters, but the borderline between viable and necrotic tissue may be diffuse due to diffusion of contrast agent from the viable tissue into the necrotic tissue. On the other hand, T_2 -weighted signal intensity images may be unsuitable for detecting tumor necrosis because the signal intensity distributions in viable and necrotic tissue are similar in some tumors.

Acknowledgements

Financial support was received from the Norwegian Cancer Society and the South-Eastern Norway Regional Health Authority.

Declaration of interest: The authors report no conflicts of interest. The authors alone are responsible for the content and writing of the paper.

References

- [1] Jain RK. Determinants of tumor blood flow: A review. *Cancer Res* 1988;48:2641–58.
- [2] Steel GG. Growth kinetics of tumors. Oxford UK: Clarendon Press; 1977.
- [3] Vaupel P, Kallinowski F, Okunieff P. Blood flow, oxygen and nutrient supply, and metabolic microenvironment of human tumors: A review. *Cancer Res* 1989;49:6449–65.
- [4] Fenton BM, Kiani MF, Siemann DW. Should direct measurements of tumor oxygenation relate to the radiobiological hypoxic fraction of a tumor? *Int J Radiat Oncol Biol Phys* 1995;33:365–73.
- [5] Verheij M. Clinical biomarkers and imaging for radiotherapy-induced cell death. *Cancer Metastasis Rev* 2008;27:471–80.
- [6] Toms AP, White LM, Kandel R, Bleakney RR, Noseworthy M, Lee S, et al. Limitations of single slice dynamic contrast enhanced MR in pharmacokinetic modeling of bone sarcomas. *Acta Radiol* 2009;50:512–20.
- [7] Jakobsen I, Kaalhus O, Lyng H, Rofstad EK. Detection of necrosis in human tumour xenografts by proton magnetic resonance imaging. *Br J Cancer* 1995;71:456–61.
- [8] Vossen JA, Buijs M, Geschwind JF, Liapi E, Prieto V, Lee KH, et al. Diffusion-weighted and Gd-EOB-DTPA-contrast-enhanced magnetic resonance imaging for characterization of tumor necrosis in an animal model. *J Comput Assist Tomogr* 2009;33:626–30.
- [9] Kettelhack C, Wickede M, Vogl T, Schneider U, Hohenberger P. ^{31}P -magnetic resonance spectroscopy to assess histologic tumor response noninvasively after isolated limb perfusion for soft tissue tumors. *Cancer* 2002;94:1557–64.
- [10] Bremer C, Bankert J, Filler T, Ebert W, Tombach B, Reimer P. High-dose Gd-DTPA vs. Bis-Gd-mesoporphyrin for monitoring laser-induced tissue necrosis. *J Magn Reson Imaging* 2005;21:801–8.
- [11] Metz S, Daldrup-Unk HE, Richter T, R ath C, Ebert W, Settles M, et al. Detection and quantification of breast tumor necrosis with MR imaging: Value of the necrosis-avid contrast agent Gadophrin-3. *Acad Radiol* 2003;10:484–90.
- [12] Benjaminsen IC, Graff BA, Brurberg KG, Rofstad EK. Assessment of tumor blood perfusion by high-resolution dynamic contrast-enhanced MRI: A preclinical study of human melanoma xenografts. *Magn Reson Med* 2004;52:269–76.
- [13] Graff BA, Benjaminsen IC, Brurberg KG, Ruud EBM, Rofstad EK. Comparison of tumor blood perfusion assessed by dynamic contrast-enhanced MRI with tumor blood supply assessed by invasive imaging. *J Magn Reson Imaging* 2005;21:272–81.
- [14] Vestvik IK, Egeland TA, Gaustad JV, Mathiesen B, Rofstad EK. Assessment of microvascular density, extracellular volume fraction, and radiobiological hypoxia in human melanoma xenografts by dynamic contrast-enhanced MRI. *J Magn Reson Imaging* 2007;26:1033–42.
- [15] Benjaminsen IC, Brurberg KG, Ruud EBM, Rofstad EK. Assessment of extravascular extracellular space fraction in human melanoma xenografts by DCE-MRI and kinetic modeling. *Magn Reson Imaging* 2008;26:160–70.
- [16] Egeland TAM, Simonsen TG, Gaustad JV, Gulliksrud K, Ellingsen C, Rofstad EK. Dynamic contrast-enhanced magnetic resonance imaging of tumors: Preclinical validation of parametric images. *Radiat Res* 2009;172:339–47.
- [17] Egeland TAM, Gaustad JV, Benjaminsen IC, Hedalen K, Mathiesen B, Rofstad EK. Assessment of fraction of hypoxic cells in human tumor xenografts with necrotic regions by dynamic contrast-enhanced MRI. *Radiat Res* 2008;169:689–99.
- [18] Tofts PS, Brix G, Buckley DL, Evelhoch JL, Henderson E, Knopp MV, et al. Estimating kinetic parameters from dynamic contrast-enhanced T_1 -weighted MRI of a diffusable tracer: Standardized quantities and symbols. *J Magn Reson Imaging* 1999;10:223–32.
- [19] Hittmair K, Gomiscek G, Langenberger K, Recht M, Imhof H, Kramer J. Method for the quantitative assessment of contrast agent uptake in dynamic contrast-enhanced MRI. *Magn Reson Med* 1994;31:567–71.
- [20] Mayr NA, Yuh WT, Arnholt JC, Ehrhardt JC, Sorosky JJ, Magnotta VA, et al. Pixel analysis of MR perfusion imaging in predicting radiation therapy outcome in cervical cancer. *J Magn Reson Imaging* 2000;12:1027–33.
- [21] Lancaster JA, Carrington BM, Sykes JR, Jones AP, Todd SM, Cooper R, et al. Prediction of radiotherapy outcome using dynamic contrast-enhanced MRI of carcinoma of the cervix. *Int J Radiat Oncol Biol Phys* 2002;54:759–67.
- [22] Morgan B, Utting JF, Higginson A, Thomas AL, Steward WP, Horsfield MA. A simple, reproducible method for monitoring the treatment of tumours using dynamic contrast-enhanced MR imaging. *Br J Cancer* 2006;94:1420–7.
- [23] Nielsen T, Murata R, Maxwell RJ, St okilde-J rgensen H, Østergaard L, Horsman MR. Preclinical studies to predict efficacy of vascular changes induced by combretastatin A-4 disodium phosphate in patients. *Int J Radiat Oncol Biol Phys* 2008;70:859–66.
- [24] Viertl D, Delaloye AB, Lanz B, Poirity-Yamate C, Gruetter R, Mlynarik V, et al. Increase of ^{18}F -FLT tumor uptake in vivo mediated by FdUrd: Toward improving cell proliferation positron emission tomography. *Mol Imaging Biol* 2010, June 16 [Epub ahead of print]. DOI: 10.1007/s11307-010-0368-z.
- [25] Mima K, Hirota M, Abe S, Iwatsuki M, Imamura H, Tsuruzoe S, et al. Small solid pseudopapillary tumor of the pancreas in a 32-year-old man: Report of a case. *Surg Today* 2010;40:772–6.
- [26] DeJordy JO, Bendel P, Horowitz A, Salomon Y, Degani H. Correlation of MR imaging and histologic findings in mouse melanoma. *J Magn Reson Imaging* 1992;2:695–700.
- [27] Lyng H, Haraldseth O, Rofstad EK. Measurement of cell density and necrotic fraction in human melanoma xenografts by diffusion weighted magnetic resonance imaging. *Magn Reson Med* 2000;43:828–36.